Journal of Molecular Structure 1253 (2022) 132286

Contents lists available at ScienceDirect

Journal of Molecular Structure

journal homepage: www.elsevier.com/locate/molstr

Determination of structural, spectral, computational and OLED properties of $Ex^{2.2}Box^{2+}$ Cyclophane and its derivatives: Experimental and computational study

Koray Sayin[a,*], Majid Rezaeivala[b,*], Sultan Erkan[a], Elif Güney[a]

[a] Department of Chemistry, Faculty of Science, Sivas Cumhuriyet University, Sivas 58140, Turkey
[b] Department of Chemical Engineering, Hamedan University of Technology, Hamedan 65155, Iran

ARTICLE INFO

Article history:
Received 9 October 2021
Revised 16 December 2021
Accepted 24 December 2021
Available online 29 December 2021

Keywords:
Ex^nBox
Cyclophane
Synthesis
Optical properties
Marcus theorem
Spectral analyses

ABSTRACT

$Ex^{2.2}Box^{2+}$ Cyclophane was synthesized, and spectral characterization of this compound was completed by using ^1H, $^{13}CNMR$, and ESI-MS spectroscopy. Furthermore, this compound and its seven derivatives were investigated by computational analyses. Initially, these compounds were optimized at B3LYP/6–31G(d) level in the gas phase and water. Then, IR and NMR spectrum were analyzed. Especially, experimental and computational results are compared with each other in $Ex^{2.2}Box^{2+}$ Cyclophane. Computational spectral results were presented due to the good harmony between experimental and computational results. These compounds' chemical reactivity and electron mobility were investigated using a contour plot of frontier molecular orbital and molecular electrostatic potential map. Finally, the OLED properties of them were examined, and it was found that compounds (**5**)–(**7**) may be suitable candidates for OLED applications.

1. Introduction

Frameworks compounds in supramolecular chemistry attract the attention of researchers due to their unique structures and interesting features [1]. Cyclophane is a family member, such as cyclodextrins, cucurbiturils, and crown ethers [2]. Cyclophanes have many application areas such as live-cell imaging, artificial molecular switches, stimulus-responsive luminescence, etc. Cyclophanes have aromatic rings bonded to aliphatic chains in a closed circuit. Both cationic structure and π electron delocalization indicate that these structures can also be used in OLED technology [3]. The Cyclophanes' optical properties are influenced by a nonconventional internal charge transfer process. Organic light-emitting diodes (OLEDs) have attracted great interest in the technology class. They have the advantages of easy manufacturing, low driving voltage, ultra-speed, high contrast ratio, low power consumption, and high brightness [4–7]. An OLED device consists of an anode and organic matter called the cathode. However, there are layers above the anode and below the cathode that determine the property of the OLED material. The electron injection layer (EIL) is located just below the cathode. Below the EIL layer is the electron transport (ETL) layer responsible for carrying electrons. There is a hole injection layer (HIL) in the upper layer of the anode. Above this layer is the hole-bearing layer (HTL), which has a good conductivity for positive charges (holes) [8].

Thanks to the applications of computational chemistry methods, the suitability of the studied compounds for the mentioned layers can be discussed with numerical results. Tetracationic Cyclophane compounds, Ex^nBox^{4+}, are produced by reacting rigid bipyridyl-based linkers, in which n is the number of p-phenylene spacers having been employed toward various chemistry [9–11]. In this study, $Ex^{2.2}BIPY$, $Ex^{2.2}DB{\bullet}2PF_6$, $Ex^{2.2}Box{\bullet}4PF_6$, and $Ex^{2.2}BIPY\text{-}Me_2{\bullet}2PF_6$ were synthesized. Especially, $Ex^{2.2}Box{\bullet}4PF_6$ and its derivatives are examined in detail. Additionally, their R and S isomers are considered for computational analyses. Their spectral characterizations are done in detail, and so they are characterized using both experimental and computational techniques. In quantum chemical calculations, the UV–VIS spectrum of them is calculated, and the wavelength of some UV bands is reported. Some quantum chemical descriptors (QCDs) are taken into account to interpret the optical properties. The calculation level is selected as B3LYP/6–31G(d) in computational analyses. OLED properties are calculated using the Marcus theorem. As a result, the investigated compounds were a good candidate for ETL, HTL, and HIL material.

* Corresponding authors.
E-mail addresses: ksayin@cumhuriyet.edu.tr (K. Sayin), mrezaeivala@gmail.com (M. Rezaeivala).

https://doi.org/10.1016/j.molstruc.2021.132286
0022-2860/

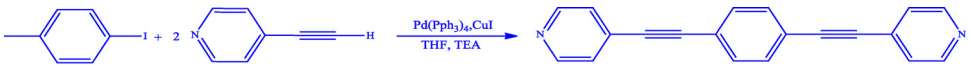

(1)

Scheme 1. Synthesis of 1,4-Bis(pyridine-4-ylethylbenzene.

2. Material and method

2.1. Synthesis

The compounds were synthesized according to literature methods [9,10].

Synthesis of 1,4-Bis(pyridine-4-ylethylbenzene, Ex$^{2.2}$BIPY (1)

$Pd(PPh_3)_4$ (0.21 g, 1.79 mmol) and CuI (0.34 g, 1.79 mmol) were suspended in 70 ml THF and TEA, and 1,4-diiodobenzene (11.8 g, 35.7 mmol) was added. The mixture was stirred for 5 min at room temperature before the addition of ethynylpyridine (10.2 g, 73.2 mmol). The reaction was stirred at 50 °C overnight under N_2. Check completion by TLC and NMR. The reaction mixture was concentrated under vacuum, diluted in H_2O/EtOAc, extracted with EtOAc, and the organic layer washed with H_2O, 1 M NaOH, and the organic layer dried and concentrated (Scheme 1). Mp: 185–186 °C. ^{1}H NMR ($CDCl_3$): 7.24 (4H, d, J = 6.0), 7.41 (4H, s), 8.48 (4H, d, J = 6.0) (Supp. Fig. S1); ^{13}C NMR ($CDCl_3$): 88.80, 93.33 9 (C = C), 122.87, 125.56, 131.19, 131.94, 149.70 (pyridine and benzene rings)(Supp. Fig. S2).

Synthesis of 4,4′-(1,4-Phenylenebis(ethyne-2,1-diyl))bis(1-(4-(bromomethyl)benzyl)pyridin-1-ium)* Bis(hexafluorophosphate)-Ex$^{2.2}$DB•2PF$_6$ *(2)

α,α'-Dibromo-p-xylene (16.38 g, 62.5 mmol) was added to $MeCN/CH_2Cl_2$ (1:1 v/v, 100 mL), and the suspension was heated at 90 °C until all of the compounds had dissolved. A suspension of Ex$^{2.2}$BIPY (1.75 g, 6.25 mmol) in $CHCl_3$ (40 mL) was added in portions over two h. After heating under reflux for 48 h, the reaction mixture was cooled to room temperature and filtered. The yellow precipitate was washed with CH_2Cl_2 (5 × 20 mL) and dissolved in a mixture of RT or warm MeOH (400 mL) and DMF (200 mL). The product was precipitated by adding NH_4PF_6 followed by diluting with cold H_2O (300 mL) and collected by filtration. Ex$^{2.2}$DB•2PF$_6$ dissolved in MeCN, filtered, and concentrated, yielding pure Ex$^{2.2}$DB•2PF$_6$ (5.20 g, 88.73%) as a yellow solid (Scheme 2). ^{1}H NMR (500 MHz, CD_3CN, ppm): δ_H 8.74 (d, J = 6.9 Hz, 4H), 8.08 (d, J = 6.9 Hz, 4H), 7.82 (s, 4H), 7.58 (d, J = 8.3 Hz, 4H), 7.45 (d, J = 8.3 Hz, 4H), 5.71 (s, 4H), 4.63 (s, 4H)(Supp. Fig. S3). ^{13C}NMR (125 MHz, CD3CN, ppm): δ_C 145.02, 140.84, 133.56, 133.40, 130.70, 130.19, 123.78, 87.78, 64.36, 33.13) (Supp. Fig. S4).

Cyclobis(4,4′-(1,4-Phenylenebis(ethyne-2,1-diyl))-bipyridin-1-ium-1,4-phenylenebis (methylene)) Tetrakis (hexafluorophosphate), Ex$^{2.2}$Box•4PF6 (3)

A solution of Ex$^{2.2}$DB•2PF$_6$ (3.34 g, 3.57 mmol) and Ex$^{2.2}$BIPY (1 g, 3.57 mmol) dry MeCN (178 mL) was stirred at RT for 48 h. The reaction was quenched by the addition of excess concentrated HCl (10 mL), whereupon the crude product precipitated from the solution as the hexachloride salt was centrifuged, washed with Me_2CO, and was dissolved in MeOH. The crude product was precipitated from solution by addition of NH_4PF_6, collected by filtration, washed with H_2O, dissolved in MeCN, and purified by crystallization from the slow vapor diffusion of iPr_2O into a solution of Ex$^{2.2}$Box•4PF$_6$ in MeCN, affording pure Ex$^{2.2}$Box•4PF$_6$ (650 mg, 29%) (Scheme 3). HRMS-ESI for Ex$^{2.2}$Box•4PF$_6$. Calcd for $C_{56}H_{40}F_{12}N_4P_2$: m/z = 529.1263 $[M\text{-}2PF_6]^{2+}$; Found: 529.1274 $[M\text{-}2PF_6]^{2+}$. ^{1}H NMR (500 MHz, CD_3CN, ppm): δ_H 8.68 (d, J = 6.9 Hz, 8H), 7.94 (d, J = 6.9 Hz, 8H), 7.67 (s, 8H), 7.58 (s, 8H), 5.67 (s, 8H)

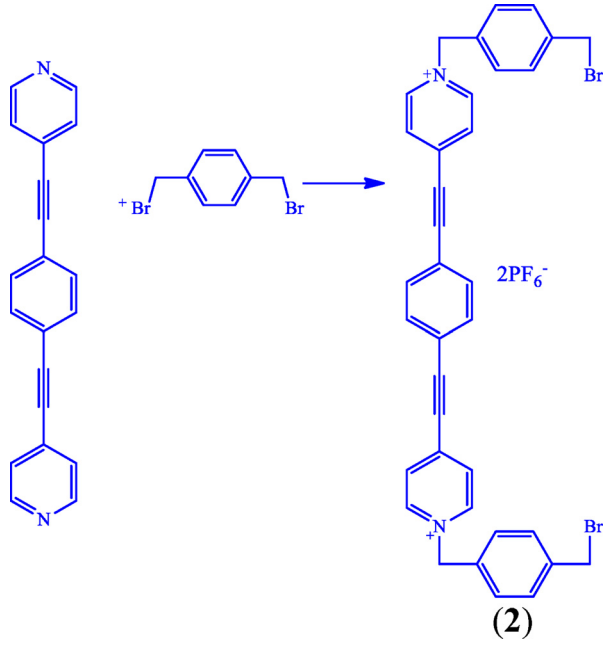

(2)

Scheme 2. Synthesis of 2.4,4′-(1,4-Phenylenebis(ethyne-2,1-diyl))bis(1-(4-(bromomethyl) benzyl)pyridin-1-ium) Bis(hexafluorophosphate).

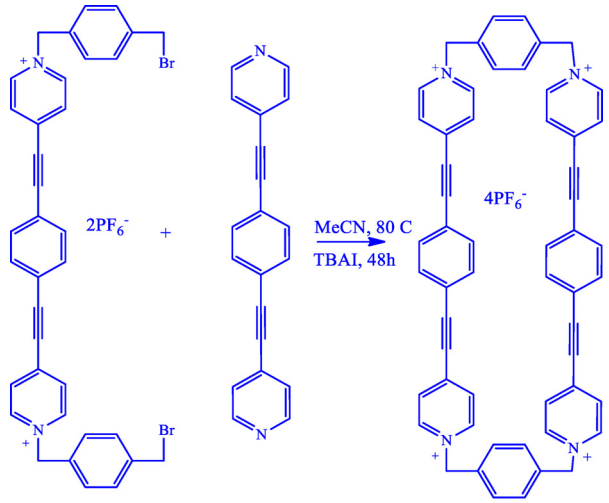

(3)

Scheme 3. Synthesis of Cyclobis (4,4′-(1,4-Phenylenebis(ethyne-2,1-diyl))-bipyridin-1-ium-1,4-phenylene bis(methylene) Tetrakis(hexafluorophosphate).

(Supp. Fig. S5). ^{13C}NMR (125 MHz, CD3CN, ppm): δ_C 144.6, 140.8, 136.1, 133.5, 131.0, 130.1, 123.2, 103.2, 87.8, 64.7 (Supp. Fig. S6).

***Synthesis of 4,4′-(1,4-phenylenebis(ethyne-2,1-diyl))bis(1-methylpyridine-1-ium) hexafluorophosphate* –Ex2.2BIPY-Me$_2$•2PF$_6$ (4)**

***Ex$^{2.2}$BIPY-Me$_2$•2PF$_6$*:** A mixture of *1,4-Bis(pyridine-4-ylethylbenzene* (50.0 mg, 0.178 mmol) and MeI (1.11 mL, 17.8 mmol) in MeCN (1.0 mL) was heated at 35 °C while stirring for 24 h. The reaction mixture was cooled to room temperature and concen-

trated *in vacuo*. The solid residue was dissolved in MeOH (20 mL), followed by the addition of an excess of NH_4PF_6 and dilution in H_2O (50 mL), resulting in the precipitation of pure **$Ex^{2.2}$BIPY-Me_2**•$2PF_6$, which was collected by filtration as a light brown solid. HRMS-ESI for $Ex^{2.2}$BIPY•$2PF_6$. Calcd for $C_{22}H_{18}F_{12}N_2P_2$: m/z = 310.3906 $[M\text{-}2PF_6]^{2+}$; Found: 309.1400 $[M\text{-}2PF_6]^{2+}$(Supp. Fig. S7). ^1H NMR (500 MHz, CD_3CN, ppm): δ_H 8.62 (d, J = 6.6 Hz, 4H), 8.07 (d, J = 6.2 Hz, 4H), 7.82 (d, J = 6.6 Hz, 4H), 4.30 (s, 6H) (Supp. Fig. S8). ^{13C}NMR (125 MHz, CD3CN, ppm): δ_C 146.4, 137.8, 130.8, 94.8, 49.3 (Supp. Fig. S9).

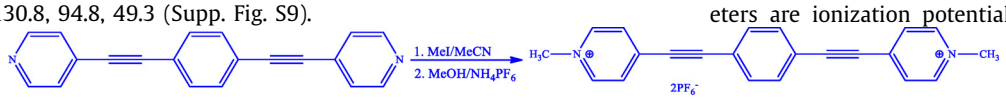

(4)

2.2. Computational approaches

Computational analyses were performed at the B3LYP method with 6–31G(d) basis set in the gas phase and water. In this project, Gaussian 5.0.8 [12], Gaussian09 AS64L-G09RevD.01 [13], and Chem-Bio Office [14] were used as software. Optimization and frequency calculations were done, and no imaginary frequency was observed. IR spectrum of related compounds and their isomers were analyzed. The peaks in the IR spectrum were labeled, and their vibration modes were declared.

The time-dependent method was used in the calculation of the UV spectrum. To consider solute-solvent interaction, the IEF-PCM method was used in the calculation. OLED properties were explained by using Marcus theory. The parameters required to examine the OLED properties of the related compounds were calculated at B3LYP/6–31G(d) level.

The compounds used in the OLED structure are classified as electron bearing layers (ETL), hole bearing layers (HTL), electron injection layer (EIL), and hole injection layer (HIL). They can be designed for these purposes [15,16]. N, N'-diphenyl-N, N'-bis (3-methylphenyl) −1,1′-diphenyl-4,4′-diamine (TPD) and tris (8-hydroxyquinoline) aluminum (III) (Alq3) respectively considered as reference material for a typical HTL and an ETL material. To predict ETL and HTL materials, a parameter that applies the Marcus theory given in Eq. (1) is taken into account.

$$K = t^2 \frac{2\pi}{\hbar} \frac{1}{\sqrt{4\pi\lambda k_B T}} exp\left[-\frac{\left(\lambda + \Delta G^0\right)^2}{4\lambda k_B T} \right] \quad (1)$$

Where T is the temperature, k_B is the Boltzmann constant. ΔG° is the free energy of the hole transfer reaction (zero in the case of a transfer of holes between identical molecules), t is the integral transfer parameter, and λ is the reorganization energies. The total reorganization energy of the molecule is equal to the sum of electron (λ_e) and hole (LH) reorganization energy.

$$\lambda = \lambda_e + \lambda_h \quad (2)$$

Reorganization energies [17], λ_e and λ_h transfer can be calculated by the following equations:

$$\lambda e = \left(E_0^- - E_-^-\right) + \left(E_-^0 - E_0^0\right) \quad (3)$$

$$\lambda h = \left(E_0^+ - E_+^+\right) + \left(E_+^0 - E_0^0\right) \quad (4)$$

where E_0^+ is the energy of the cation calculated with the optimized structure of the neutral molecule, E_0^- is the energy of the anion calculated with the optimized structure of the neutral molecule. E_+^+ and E_-^- are the energy of the cation and anion, respectively. E_+^0 is the energy of the neutral molecule calculated at the cationic state. (E_-^0) is the energy of the neutral molecule calculated at the anionic state. E_0^0 is the energy of the neutral molecule at the ground state [18].

Typical ETL and HTL materials are evaluated with reorganization data in the literature. In evaluation, Alq3 and TPD compounds are taken as reference. The electron reorganization energy (λ_e) of Alq3 has been reported at 0.276 eV [11] and the hole reorganization energy (LH) of TPD at 0.290 eV [19].

In addition, two basic parameters are examined in EIL and HIL materials that determine the ease of charge transfer. These parameters are ionization potentials (IPs) and electron affinities (EAs). Lower IP and higher EA mean better hole and electron transport. In other words, smaller IP (larger EA) values indicate easier injection of holes from the transport layer of the holes (electrons) to the emitter layers. [20] Ionization potential (IP_a), vertical ionization potential (IPV), adiabatic electron affinity (EA_a), and vertical electron affinity (EA_v) are calculated as follows.

$$IP_a = E_+ - E_0^0 \quad (5)$$

$$IP_v = E_0^+ - E_0^0 \quad (6)$$

$$EA_a = E_0^0 - E_- \quad (7)$$

$$EA_v = E_0^0 - E_0^- \quad (8)$$

here, E_0^- (E_0^+) is the energy of the anion (cation) calculated with the optimized structure of the neutral molecule. E_-(E_+) is the energy of the anion (cation) calculated with the optimized anion (cation) structure [21].

3. Result and discussion

3.1. Structures at ground state and simulated characterization

$Ex^{2.2}Box^{4+}$ and its additive derivatives are optimized at B3LYP/6–31G(d) level in the gas phase and water. Optimized structures of studied compounds in the gas phase and their labeling are represented in Fig. 1. Additionally, optimized structures in water are given in Supplemental Figs. S10–S17.

Given the optimized structure of studied molecules, the whole compounds are quite tense. There are many π electrons. Molecular planarity is distorted in each compound. Especially, benzene rings on both sides are nearly perpendicular to other benzene rings. IR spectrum of each studied compound was calculated, and no imaginary frequency was observed in the results. IR spectrum of studied compounds was examined, and the labeled IR spectrum in both phases is given in Supp. Figs. S18–S33. The analyses of the labeled peak in the IR spectrum are given in Table 1.

According to Table 1, vibrational frequencies of some functional groups and specific bonds such as double and triple are observed in detail. The triple bond between carbon atoms is calculated in the range of 2290 - 2280 cm^{-1}, while the stretching frequency of the double bond is calculated in the range of 1590 – 1710 cm^{-1}. As for the CH stretching frequency, CH stretching frequencies are observed in compound (**3**) and (**5**)–(**7**) while the intensity of these frequencies is too small. Therefore, it is accepted as not observed in the IR spectrum. On the other hand, the NMR spectrum of studied compounds is calculated and evaluated using TMS. The calculated chemical shift values of carbon and hydrogen atoms are given in Table 2.

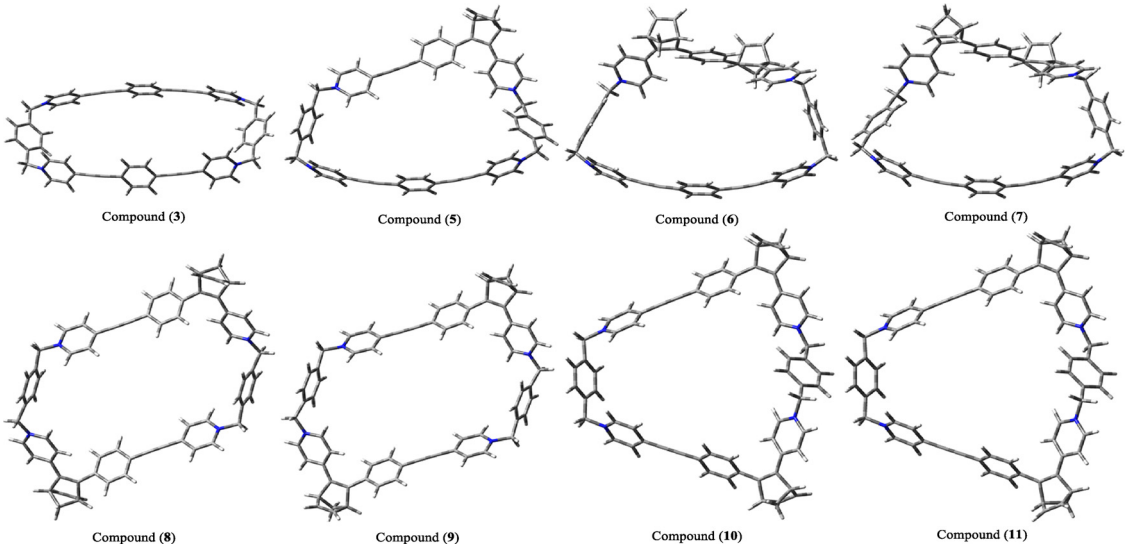

Fig. 1. Ground state structure of studied of some $Ex^{2.2}Box^{4+}$ Cyclophanes and their additive derivatives.

Table 1
The analyses of labeled peaks of related IR spectrum.

Assignment	Comp (**3**) [a]	Comp (**5**) [a]	Comp (**6**) [a]	Comp (**7**) [a]
1	3218 > STRE ($CH_{aro.}$)	3236 > STRE ($CH_{aro.}$)	3234 > STRE ($CH_{aro.}$)	3238 > STRE ($CH_{aro.}$)
2	3044 > STRE ($CH_{alp.}$)	3063 > STRE ($CH_{alp.}$)	3059 > STRE ($CH_{alp.}$)	3053 > STRE ($CH_{alp.}$)
3	2191 > STRE (C≡C)	2190 > STRE (C≡C)	2191 > STRE (C≡C)	2189 > STRE (C≡C)
4	1708 > STRE (C=C)	1711 > STRE (C=C)	1712 > STRE (C=C)	1712 > STRE (C=C)
5	1222 > BEND (CH)	1202 > STRE (CN), BEND (CH)	1171 > STRE (CN), BEND (CH)	1173 > STRE (CN), BEND (CH)
Assignment	Comp (**8**) [a]	Comp (**9**) [a]	Comp (**10**) [a]	Comp (**11**) [a]
1	2281 > STRE (C≡C)	2281 > STRE (C≡C)	2282 > STRE (C≡C)	2282 > STRE (C≡C)
2	1682 > STRE (C=C)	1682 > STRE (C=C)	1682 > STRE (C=C)	1685 > STRE (C=C)
3	1598 > STRE (C=C)	1598 > STRE (C=C)	1593 > STRE (C=C)	1593 > STRE (C=C)
4	1141 > BEND (CH)	1142 > STRE (CN), BEND (CH)	1153 > STRE (CN), BEND (CH)	1147 > STRE (CN), BEND (CH)

[a] Frequency is given in cm^{-1}, STRE and BEND mean stretching and bending mode, respectively.

Table 2
Calculated chemical shift values (ppm) of carbon and hydrogen atoms of studied compounds.

For ^{13}C NMR Assignment	Comp (**3**)	Comp (**5**)	Comp (**6**)	Comp (**7**)	Comp (**8**)	Comp (**9**)	Comp (**10**)	Comp (**11**)
Aromatic Carbon	133 - 105	132 - 105	133 - 106	133 - 105	148 - 114	149 - 114	149 - 118	148 - 118
Aliphatic Carbon	57	59 - 56	58 - 56	58 - 56	67 - 64	73 - 63	74 - 62	73 - 63
Bicyclo[2.2.1] hepta-2,5-diene	–	57 - 51	53 - 50	54 - 50	63 - 58	60 - 58	59 - 57	61 - 57
For ^{1}H NMR								
Aromatic Carbon	7.9 - 5.3	7.8 - 5.1	7.5 - 5.1	7.7 - 5.1	8.2 - 7.0	8.2 - 7.0	8.2 - 6.7	8.3 - 6.7
Aliphatic Carbon	3.9 - 3.7	4.1 - 3.7	4.2 - 3.7	4.2 - 3.7	5.3 - 5.1	5.3 - 5.1	5.4 - 5.0	5.4 - 4.9
Bicyclo[2.2.1] hepta-2,5-diene	–	3.5 - 1.6	3.4 - 1.6	3.5 - 1.6	4.0 - 2.7	4.2 - 2.7	4.2 - 2.7	4.1 - 2.6

The experimental and calculated chemical shift values of carbon and hydrogen atoms of compound (**3**) are compared with each other. In ^{1}H NMR, four NMR peaks are observed, and they are coordinated to aromatic carbon atoms. The experimental peaks are supported with computational results. Additionally, the other hydrogen atoms are characterized using computational results. As for the carbon atoms in compound (**3**), experimentally observed peaks belong to aromatic and aliphatic carbon atoms. At computational calculations, similar chemical shift values for aromatic and aliphatic carbon atoms are observed. According to NMR calculations, structures are characterized using obtained results.

3.2. Contour plots and molecular electrostatic potential (MEP) map

Detecting active sites or regions on the molecular structure is crucial to explaining the interactions. There are some ways to explain this property: contour plots of molecular orbitals, MEP maps, etc. Electron mobility and electron localization are significant. In the determination of molecular reactivity, the energy of the highest occupied molecular energy (HOMO), energy of the lowest unoccupied molecular orbital (LUMO), and the energy gap between LUMO and HOMO (E_{GAP}) are important parameters. Additionally, electron localization regions provide significant clues about the active region on the molecular structure. Therefore, contour plots of HOMO are calculated and represented in Fig. 2 to explain the electron mobility. Contour plot of frontier molecular orbital in water phase are given in Supp. Figs. S34–S49 for studied compounds.

According to Fig. 2, electron delocalization in compound (3)–(7) is more on the whole structure than other compounds in compound (3)–(7) is more than those of the others. Due to the high electron mobility, these molecules are expected to have high OLED properties. Therefore, it is also expected to exhibit better OLED properties than other compounds. Molecular electrostatic potential (MEP) maps are calculated for each compound and represented in Fig. 3. MEP maps of studied compounds in the water phase are given in Supp. Figs. S50–S57.

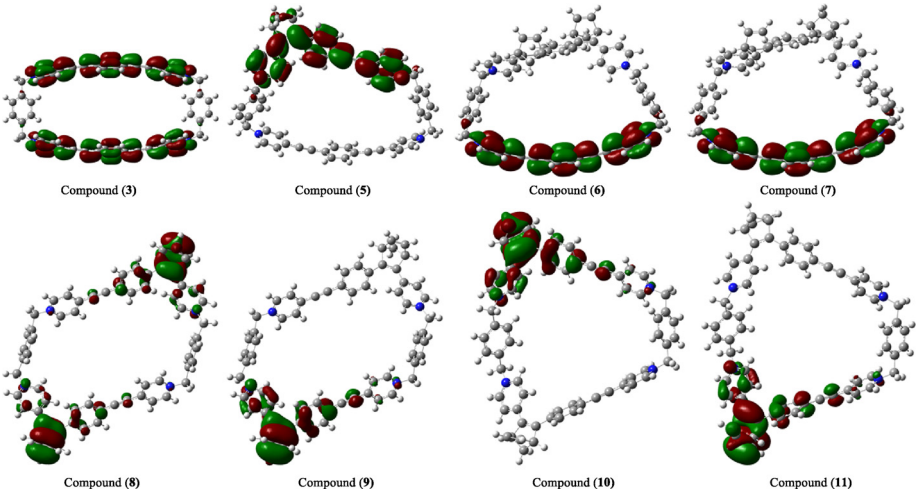

Fig. 2. The contour plots of HOMO of each studied compound.

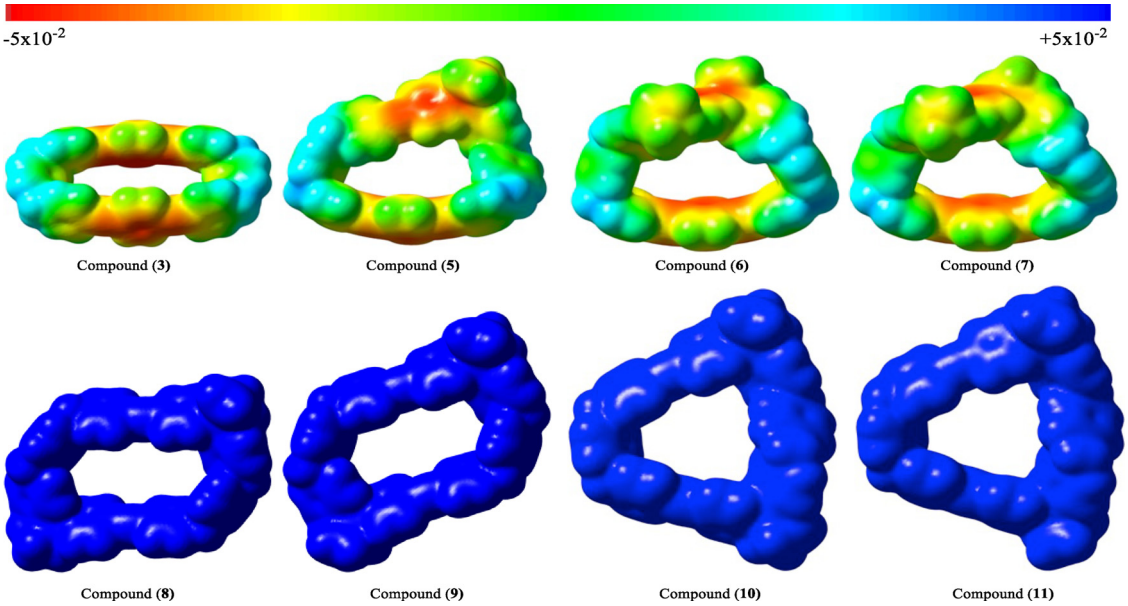

Fig. 3. MEP maps of each compound.

According to Fig. 3, electron delocalization are mainly on the surface at compound (**3**)–(**7**). There are different electron density regions on these compounds, while the color is blue on the surface of compound (**8**)–(**11**). As a result, the electron mobility compound (**3**) – (**7**) is more than others. Furthermore, the chemical reactivity is more in the first four compounds. These results imply that the OLED properties of compound (**3**), (**5**)–(**7**) can be more than those of other compounds.

3.3. Calculated UV–VIS spectrum

UV–VIS spectrum is an effective technique for determining electron mobility in the molecule. For this aim, the UV–VIS spectrum of studied compounds is calculated at the same level of theory in three different mediums, chloroform (ε=4.7113), DMSO (ε=46.826) and water (ε=78.3553). The wavelength of the bands is given in Table 3.

According to Table 3, the wavelengths of the main bands are different from each other. The required energy for the electronic transition decreases with the increasing of the wavelength. Therefore, the less required energy for electron mobility can be occurred in compound (3), (5), and (6). For those reasons, OLED properties can be well in these compounds.

3.4. OLED properties

The reorganization energy, the adiabatic and vertical ionization potentials (IP_a/IP_v), and electron affinities (EA_a/EA_v) parameters were calculated so that the studied Ex2.2Box4+ and its additive derivatives could be seen as electron bearing layers (ETL), hole bearing layers (HTL), electron injection layer (EIL) and hole injection layer (HIL). The calculated values of the reorganization energy, the adiabatic and vertical ionization potentials (IP_a/IP_v), and electron affinities (EA_a/EA_v) (in eV) for all examined compounds are listed in Table 4.

In order for an organic compound to be suitable as ETL material, λ_e values must be less than 0.276 eV. Likewise, in order for the organic compound to be the suitable material for the HTL layer, the LH values must be less than 0.290 eV. Finally, the charge transfer property of EIL and HIL materials can be evaluated with IPa, IPv, and EAa, EAv results, respectively. Lower IP and higher EA mean better electrons and holes charge transfer, respectively [20].

Table 3
The wavelength (nm) of the observed bands in the UV–VIS spectrum in different areas.

Compounds	Area	Main Band	Band
(3)	Chloroform	670	353
	DMSO	661	351
	Water	646	350
(5)	Chloroform	684	378
	DMSO	678	375
	Water	663	374
(6)	Chloroform	682	361
	DMSO	676	359
	Water	662	358
(7)	Chloroform	677	358
	DMSO	471	356
	Water	466	359
(8)	Chloroform	385	–
	DMSO	470	362
	Water	450	–
(9)	Chloroform	445	
	DMSO	453	–
	Water	446	–
(10)	Chloroform	440	–
	DMSO	450	–
	Water	352	–
(11)	Chloroform	362	–
	DMSO	355	470
	Water	468	352

Table 4
Calculated reorganization energies (in eV), the adiabatic and vertical ionization potentials (IPa/IPv), and electron affinities (EAa/EAv) (in eV) for all compounds.

Complex	IP_a	IP_v	EA_a	EA_v	λ_e	λ_h
(**3**)	0.3558	0.2362	0.2069	0.2026	1.42	1.60
(**5**)	0.1427	0.1383	0.1216	0.1757	0.17	0.16
(**6**)	0.1619	0.1505	0.1346	0.1332	0.20	0.19
(**7**)	0.1448	0.1412	0.1590	0.1632	0.21	0.10
(**8**)	0.1449	0.1411	0.2289	0.2333	0.10	0.14
(**9**)	0.1531	0.1384	0.2502	0.2535	0.11	0.13
(**10**)	0.1653	0.1107	0.3513	0.3524	0.12	0.13
(**11**)	0.1756	0.1089	0.3519	0.3542	0.14	0.12

When the λ_e and λ_h values of organic compounds in Table 1 are examined, it is seen that the values of λ_e are lower than 0.276 eV, and the values of λ_h are 0.290 eV. So, in OLED materials where π-electron delocalization is very important, the studied compounds meet the expectation. All compounds are suitable for use as both ETL and HTL material. This also means that the same compound can be used in two layers in an OLED material. In Table 1, a remarkable point in reorganization energies is that compound (**6**), (**8**), and (**10**) have low λ_e values and high LH values from compound (**7**), (**9**), and (**11**). When the IPs and EA's in Table 1 are examined, the IPs of all the compounds except compound (**3**) are increasingly decreasing, and their EAs are increasing. Primarily, compound (**5**)–(**7**) can be used as material for both HIL and EIL layers.

4. Conclusion

We presented the synthesis and computational investigations of some $Ex^{2.2}Box^{2+}$ Cyclophane derivatives. Spectral characterization of $Ex^{2.2}Box$ is done experimentally. Additionally, quantum chemical calculations are performed at B3LYP/6–31G(d) level. $Ex^{2.2}Box^{2+}$ Cyclophane and its seven additive derivative structures are examined in detail. Their optimization and simulated spectral characterization are done, and some data are compared with experimental results. Contour plots and MEP maps examine studied compounds' chemical reactivity and conductivity. Finally, their OLED properties are investigated using the Marcus theorem. It is found that OLED properties of compound (**5**)–(**7**) are more than those of others. It can be said that compound (**5**), (**6**), and (**7**) may be suitable candidates for OLED applications.

Declaration of Competing Interest

The authors declare that they have no known competing financial interests or personal relationships that could have appeared to influence the work reported in this paper.

CRediT authorship contribution statement

Koray Sayin: Formal analysis, Writing – review & editing, Software. **Majid Rezaeivala:** Formal analysis, Writing – review & editing, Methodology. **Sultan Erkan:** Formal analysis, Writing – review & editing, Software. **Elif Güney:** Writing – original draft, Writing – review & editing, Software.

Acknowledgments

The numerical calculations reported in this paper were fully/partially performed at TUBITAK ULAKBIM, High Performance and Grid Computing Center (TRUBA resources). Also, M. R thanks Professor Sir J. Fraser Stoddart for giving me the opportunity to learn this field of Chemistry during the sabbatical time at Northwestern University in 2016.

Supplementary materials

Supplementary material associated with this article can be found, in the online version, at doi:10.1016/j.molstruc.2021.132286.

References

[1] S. Kotha, M.E. Shirbhate, Design of new synthetic strategies to Cyclophanes via ring-closing metathesis, Tetrahedron Lett. 55 (2014) 6972–6975.
[2] S.S.M. Sundaram, S. Karthick, K. Sailaja, R. Karkuzhali, G. Gopu, Theoretical study on Cyclophane amide molecular receptors and its complexation behavior with TCNQ, J. Photochem. Photobiol. B Biol. 203 (2020) 111735.
[3] R.C. Evans, P. Douglas, C.J. Winscom, Coordination complexes exhibiting room-temperature phosphorescence: evaluation of their suitability as triplet emitters in organic light-emitting diodes, Coord. Chem. Rev. 250 (2006) 2093–2126.
[4] C.W. Ko, Y.T. Tao, Bright white organic light-emitting diode, Appl. Phys. Lett. 79 (2001) 4234–4236.
[5] J. Li, L. Hu, L. Wang, Y. Zhou, G. Grüner, T.J. Marks, Organic light-emitting diodes having carbon nanotube anodes, Nano Lett. 6 (11) (2006) 2472–2477.
[6] M.R. Krames, H. Amano, J.J. Brown, P.L. Heremans, Introduction to the issue on high-efficiency light-emitting diodes, J. Sel. Top. Quantum Electron. 8 (2) (2002) 185–188.
[7] N.L. Liu, N. Ai, D.G. Hu, S.F. Yu, J.B. Peng, Y. Cao, J. Wang, Effect of spin-coating process on the performance of passive-matrix organic light-emitting display, Acta Phys. Sin. 60 (8) (2011) 087805.
[8] R. Ma, Organic light-emitting diodes (OLEDs), in: Handbook of Visual Display Technology, in: Handbook of Visual Display Technology, 2, Springer, 2016, pp. 1209–1221.
[9] E.J. Dale, N.A. Vermeulen, M. Juricek, J.C. Barnes, R.M. Young, M.R. Wasielewski, J.F. Stoddart, Supramolecular explorations: exhibiting the extent of extended cationic cyclophanes, Acc. Chem. Res. 49 (2016) 262–273.
[10] E.J. Dale, D.P. Ferris, N.A. Vermeulen, J.J. Hanks, I. Popovs, M. Juricek, J.C. Barnes, S.T. Schneebeli, J.F. Stoddart, Cooperative reactivity in an extended-viologen-based cyclophane, J. Am. Chem. Soc. 138 (2016) 3667–3670.
[11] K. Sayin, M. Rezaeivala, Modelling studies on the investigation of non-linear optical properties of some Ex^nBox Cyclophanes, Cumhur. Sci. J. 41 (2) (2020) 344–350.
[12] R.D. Dennington, T.A. Keith, J.M. Millam, GaussView 5.0, Wallingford, CT, 2009.
[13] M.J. Frisch, G.W. Trucks, H.B. Schlegel, et al., Gaussian 09, Revision D.01 Scuseria G. E., Robb M. A., Cheeseman J. R., Scalmani G., Barone V., Petersson G. A., Nakatsuji H., Li X., Caricato M., Marenich A. V., Bloino J., Janesko B.G., Gomperts R., Mennucci B., Hratchian H. P., Ortiz J. V., Izmaylov A. F., Sonnenberg J. L., Williams-Young D., Ding F., Lipparini F., Egidi F., Goings J., Peng B., Petrone A., Henderson T., Ranasinghe D., Zakrzewski V. G., Gao J., Rega N., Zheng G., Liang W., Hada M., Ehara M., Toyota K., Fukuda R., Hasegawa J., Ishida M., Nakajima T., Honda Y., Kitao O., Nakai H., Vreven T., Throssell K., Montgomery J.A. Jr., Peralta J. E., Ogliaro F., Bearpark M.J., Heyd J.J., Brothers E.N., Kudin K.N., Starovero, V.N., Keith T.A., Kobayashi R., Normand J., Raghavachari K., Rendell A.P., Burant J.C., Iyengar S.S., Tomasi J., Cossi M., Millam J.M., Klene M., Adamo C., Cammi R., Ochterski J.W., Martin R.L., Morokuma K., Farkas O., Foresman J. B. and Fox D. J., Gaussian, Inc., Wallingford CT, 2009.

[14] PerkinElmerChemBioDraw Ultra Version (13.0.0.3015), CambridgeSoft, Waltham, MA, USA, 2012.
[15] C.W. Kim, J.H. Lee, S. Cho, H.J. Kim, J. Hwang, Y.W. Kim, D.H. Choi, Novel carbazole-acridine-based hole transport polymer for low turn-on voltage of green quantum dot light-emitting diodes, Polym. Chem. 12 (32) (2021) 4714–4721.
[16] Y. Zheng, J. Huo, S. Xiao, H. Shi, D. Ma, B.Z. Tang, Synthesis, photoluminescence and electroluminescence properties of a new blue emitter containing carbazole, acridine and diphenyl sulfone units, Org. Electron. 101 (2021) 106411.
[17] A.K. Chauhan, P. Jha, D.K. Aswal, J.V. Yakhmi, Organic devices: fabrication, applications, and challenges, J. Electron. Mater. (2021), doi:10.1007/s11664-021-09338-0.
[18] S. Erkan, Activity of the rocuronium molecule and its derivatives: a theoretical calculation, J. Mol. Struct. 1189 (2019) 257–264.
[19] G.A. Chamberlain, Organic solar cells: A review, Solar Cells 8 (1) (1983) 47–83.
[20] K. Nehra, A. Dalal, A. Hooda, S. Bhagwan, R. K.Saini, B. Mari, D. Singh, Lanthanides β-diketonate complexes as energy-efficient emissive materials: a review, J. Mol. Struct. 1249 (2021) 131531.
[21] A. Üngördü, Electronic, optical, and charge transfer properties of porphyrin and metallated porphyrins in different media, Int. J. Quantum Chem. 120 (6) (2020) e26128.